NACA

RESEARCH MEMORANDUM

AERODYNAMIC CHARACTERISTICS OF A WING WITH UNSWEPT QUARTER-CHORD LINE, ASPECT RATIO 4, TAPER RATIO 0.6, AND NACA 65A004 AIRFOIL SECTION

TRANSONIC-BUMP METHOD

By Boyd C. Myers, II, and James W. Wiggins

Langley Aeronautical Laboratory
Langley Air Force Base, Va.

NATIONAL ADVISORY COMMITTEE
FOR AERONAUTICS

WASHINGTON

May 8, 1950

NATIONAL ADVISORY COMMITTEE FOR AERONAUTICS

RESEARCH MEMORANDUM

AERODYNAMIC CHARACTERISTICS OF A WING WITH UNSWEPT QUARTER-CHORD LINE, ASPECT RATIO 4, TAPER RATIO 0.6, AND NACA 65A004 AIRFOIL SECTION

TRANSONIC-BUMP METHOD

By Boyd C. Myers, II, and James W. Wiggins

SUMMARY

As part of a transonic research program conducted by the National Advisory Committee for Aeronautics, a series of wing-body combinations is being investigated in the Langley high-speed 7- by 10-foot tunnel over a Mach number range of 0.60 to 1.15 utilizing the transonic-bump technique.

This paper presents the results of the investigation of a wing alone and a wing-fuselage combination employing a wing with an unswept quarter-chord line, aspect ratio 4, taper ratio 0.6, and an NACA 65A004 airfoil section. Lift, drag, pitching moment, and root bending moment were obtained for these configurations. Effective downwash angles and dynamic-pressure characteristics were also obtained for these configurations for a range of tail heights in the region of a probable tail location. In order to expedite the publication of these data, only a brief analysis is included.

INTRODUCTION

A series of wings is being investigated in the Langley high-speed 7- by 10-foot tunnel to study the effects of wing geometry on the wing alone and wing-fuselage longitudinal stability characteristics at transonic speeds. The same fuselage is used for all wings tested in this series. A Mach number range between 0.60 and 1.15 is obtained by utilizing the transonic-bump technique.

This paper presents the results of the investigation of the wing alone and of the wing-fuselage configurations employing a wing with an unswept quarter-chord line, aspect ratio 4, taper ratio 0.6, and an NACA 65A004 airfoil section parallel to the air stream. The experimental results of a wing of identical plan form having an NACA 65A006 airfoil section which was tested as part of the transonic program are presented in reference 1.

SYMBOLS

C_L lift coefficient (Twice semispan lift/qS)

C_D drag coefficient (Twice semispan drag/qS)

C_m pitching-moment coefficient referred to $0.25\bar{c}$ (Twice semispan pitching moment/$qS\bar{c}$)

C_B bending-moment coefficient at plane of symmetry $\left(\text{Root bending moment}/q\,\frac{S}{2}\,\frac{b}{2}\right)$

q effective dynamic pressure over span of model, pounds per square foot $\left(\frac{1}{2}\rho V^2\right)$

S twice wing area of semispan model, 0.125 square foot

$\bar{c}$ mean aerodynamic chord (M.A.C.) of wing, 0.181 foot $\left(\frac{2}{S}\int_0^{b/2} c^2 dy \text{ (using theoretical tip)}\right)$

c local wing chord, feet

b twice span of semispan model

y spanwise distance from plane of symmetry

ρ air density, slugs per cubic foot

V airspeed, feet per second

M effective Mach number over span of model

M_l local Mach number

M_a average local Mach number, chordwise

R Reynolds number of wing based on $\bar{c}$

α angle of attack, degrees

ϵ effective downwash angle, degrees

q_{wake}/q ratio of point dynamic pressure to free-stream dynamic pressure

y_{cp} lateral center of pressure, percent semispan $\left(100\frac{\partial C_B}{\partial C_L}\right)$

h_t tail height relative to wing chord plane extended, percent semispan, positive for tail positions above chord plane extended

MODEL AND APPARATUS

The wing of the semispan model had 0° sweepback referred to the quarter-chord line, a taper ratio of 0.60, an aspect ratio of 4, and an NACA 65A004 airfoil section parallel to the free stream. The wing was made of steel and the fuselage of brass. A two-view drawing of the model is presented in figure 1, and ordinates of the fuselage of fineness ratio 10 can be found in table I.

The model was mounted on an electrical strain-gage balance which was enclosed in the bump, and the lift, drag, pitching moment, and bending moment about the model plane of symmetry were measured with potentiometers.

Effective downwash angles were determined for a range of tail height by measuring the floating angles of free-floating tails with the aid of calibrated galvanometers. Details of the floating tails are shown in figures 2 and 3, and a pictorial view of the model on the bump, showing three of the floating tails, is given in figure 4. The tails used in this investigation were of the same geometry as those used in reference 1.

A total-pressure rake was employed to determine point dynamic-pressure ratios for a range of tail heights along a line which contained the 25-percent-mean-aerodynamic-chord point of the free-floating tails. The total-pressure tubes were spaced 1.8 inch apart near the wing-chord line extended and 1/4 inch apart elsewhere.

TESTS

The tests were made in the Langley high-speed 7- by 10-foot tunnel utilizing an adaptation of the NACA wing-flow technique for obtaining transonic speeds. The technique used involves placing the model in the high-velocity flow field generated over the curved surface of a bump on the tunnel floor. (See reference 2.)

Typical contours of local Mach number in the vicinity of the model location on the bump, obtained from surveys with no model in position, are shown in figure 5. There is a Mach number variation of about 0.05 over the model semispan at the lower Mach numbers and from 0.07 to 0.08 at the higher Mach numbers. The chordwise Mach number variation is generally less than 0.01. No attempt has been made to evaluate the effects of this chordwise and spanwise Mach number variation. Note that the long-dash lines shown near the root of the wing (fig. 5) represent a local Mach number 5 percent below the maximum value and indicate the extent of the bump boundary layer. The effective test Mach number was obtained from contour charts similar to those presented in figure 5 using the relationship

$$M = \frac{2}{S} \int_0^{b/2} cM_a \, dy$$

The variation of mean test Reynolds number with Mach number is shown in figure 6. The boundaries in the figure indicate the range in Reynolds number caused by variations in atmospheric test conditions in the course of the investigation.

Force and moment data, effective downwash angles, and the ratio of dynamic pressure at 25 percent of the mean aerodynamic chord of the free-floating tails to free-stream dynamic pressure were obtained for the model wing alone and wing-fuselage configurations tested through a Mach number range of 0.60 to 1.15 and an angle-of-attack range of about -4° to 10°.

The end-plate tare corrections to the drag and to the downwash data were obtained through the test Mach number range at 0° angle of attack by testing the model configurations without end plates. To minimize leakage a gap of about 1/16 inch was maintained between the wing root chord and the bump surface, and a sponge wiper seal (see fig. 7) was fastened to the wing butt beneath the surface of the bump. The end-plate tares have been found to be constant with angle of attack, and the tares obtained at zero angle of attack were applied to all drag and downwash data. No end-plate tare corrections were applied to other force and moment data presented, since they were found to be very small

for this model. Jet-boundary corrections have not been evaluated because the boundary conditions to be satisfied are not rigorously defined. However, inasmuch as the effective flow field is large compared with the span and chord of the model, the corrections are believed to be small. No base-pressure correction has been applied to the wing-fuselage drag data.

By measuring tail-floating angles without a model installed, it was previously determined that a tail spacing of 2 inches relative to wing chord plane would produce negligible interference effects on the tail-floating angles. Downwash angles for the wing alone configuration were therefore obtained simultaneously for the middle, highest, and lowest tail positions in one series of tests and simultaneously for the two intermediate positions in succeeding runs. (See fig. 3.) For the wing-fuselage tests, the effective downwash angles at the chord plane extended were determined by mounting a free-floating tail on the center line of the fuselage. The downwash angles presented are increments from the tail-floating angles without a model in position. It should be noted that the tail-floating angles presented are a measure of the angle of zero pitching moment about the tail-pivot axis rather than the angle of zero lift. It has been estimated, however, that for this tail arrangement a downwash gradient as large as 2° across the span of the tail will result in an error of about 0.2° in the measured downwash angle.

The total-pressure readings were obtained at constant angles of attack through the Mach number range without an end plate on the model to eliminate end-plate wakes and with the support-strut gap sealed with a foam-rubber seal to minimize any strut-leakage effects. The static-pressure values used in computing the dynamic-pressure ratios were obtained by use of a static probe with no model in position.

RESULTS AND DISCUSSION

A table of the figures presenting the results follows:

	Figure
Wing alone force data	8
Wing-fuselage force data	9
Effective downwash angles (wing alone configuration)	10
Effective downwash angles (wing-fuselage configuration)	11
Downwash gradients	12
Dynamic-pressure surveys	13
Summary of aerodynamic characteristics	14

The discussion is based on the summarized values given in figure 14 unless otherwise noted. The slopes summarized in figure 14 have been averaged over a lift-coefficient range of ±0.1.

Lift and Drag Characteristics

The lift-curve slope of the isolated wing measured near zero lift was about 0.072 at a Mach number of 0.60. This value compares favorably with a value of 0.073 estimated for this Mach number by using the low-speed semispan data at high Reynolds number from reference 3 for a model with the same plan form and with an NACA 65A006 airfoil section and by applying a compressibility correction as outlined in reference 4. Experimental results of a geometrically identical wing plan form with an NACA 65A006 airfoil section tested on the transonic bump indicated a wing lift-curve slope of about 0.074 for this Mach number (reference 1). It should be noted, however, that for the wing of the present report the maximum value of lift-curve slope near zero lift was about 0.103 at $M = 0.93$ which is about 15 percent greater than that for the wing of reference 1. In addition, the wing of the present report had a gradual single-peaked variation of $\frac{\partial C_L}{\partial \alpha}$ with M at Mach numbers above force break as contrasted with the twin-peaked variation obtained for the thicker wing of reference 1. The addition of the fuselage had little or no effect throughout the Mach number range.

Drag rise at zero lift occurred at a Mach number of about 0.91 for both the wing alone and wing-fuselage configurations. Wing alone minimum drag coefficient was 0.005 at $M = 0.60$ and rose to a maximum value of about 0.022 at the highest Mach numbers. This value of minimum drag coefficient of 0.022 at $M = 1.10$ is about one-half that obtained at the same Mach number for the wing of reference 1. The addition of the fuselage increased the value of minimum drag coefficient at the lowest Mach number to about 0.018 and to about 0.042 at the highest Mach number.

The lateral center-of-pressure location of about 44 percent semispan was practically constant through the Mach number range for the wing alone configuration. This value of $y_{cp} = 0.44$ compares with a value of about 0.43 as predicted from the theory of reference 4. The addition of the fuselage moved the lateral center of pressure inboard about 2 percent of the semispan at low Mach numbers and about 1 percent of the semispan at high Mach numbers.

Pitching-Moment Characteristics

Near zero lift the wing alone aerodynamic center was located at 25 percent mean aerodynamic chord $\left(\left(\frac{\partial C_m}{\partial C_L}\right)_M = 0\right)$ for Mach numbers up to 0.85. This aerodynamic-center location compares with a value of

24 percent mean aerodynamic chord at $M = 0.60$ for the thicker wing of identical plan form of reference 1. Above a Mach number of 0.85, the aerodynamic center of the wing of this paper moves back with increasing M to about 39 percent mean aerodynamic chord at Mach numbers above 1.05. The addition of the fuselage moved the aerodynamic-center location forward about 8 percent of the mean aerodynamic chord at low Mach numbers and about 6 to 7 percent of the mean aerodynamic chord at Mach numbers above $M = 0.85$.

Downwash and Dynamic-Pressure Surveys

The downwash gradients $\left(\frac{\partial\epsilon}{\partial\alpha}\right)_M$ near zero lift for the wing alone and wing-fuselage configurations were a maximum at the chord plane extended throughout the Mach number range (fig. 12). From figure 14 it should be noted that the variation of $(\partial\epsilon/\partial\alpha)$ with Mach number for tail heights of 0 and ±30 percent semispan was similar to the variation of the lift-curve slope with Mach number except for the one instance $h_t = 0$ for the wing alone configuration where $\partial\epsilon/\partial\alpha$ remained constant above $M = 0.93$.

The results of the point dynamic-pressure surveys made along a line containing the 25-percent-mean-aerodynamic-chord points of the free-floating tails used in the downwash surveys are presented in figure 13. Below a Mach number of 1.00 there was little difference in the wake characteristics between the wing alone and wing-fuselage configurations except that slightly larger wake losses are indicated for the wing fuselage at $\alpha = 10^{\circ}$. At Mach numbers of unity and greater and for $\alpha = 10^{\circ}$ the wake losses for the wing-fuselage configuration were more extensive and of much greater intensity than the wake losses for the wing alone. It should be noted, however, that the surveys were obtained in only one spanwise location. Similar wake behavior was also found to exist for the wing alone and the wing-fuselage configurations of reference 1 and the results of additional spanwise surveys reported in reference 1 indicated a very large spanwise dynamic-pressure gradient near the fuselage that was not present for the isolated-wing configuration. The reasons for such flow conditions are not understood but it is suggested that similar conditions probably exist on the present wing-fuselage combination.

Langley Aeronautical Laboratory
National Advisory Committee for Aeronautics
Langley Air Force Base, Va.

REFERENCES

1. Goodson, Kenneth W., and Morrison, William D., Jr.: Aerodynamic Characteristics of a Wing with Unswept Quarter-Chord Line, Aspect Ratio 4, Taper Ratio 0.6, and NACA 65A006 Airfoil Section. Transonic-Bump Method. NACA RM L9H22, 1949.

2. Schneiter, Leslie E., and Ziff, Howard L.: Preliminary Investigation of Spoiler Lateral Control on a 42° Sweptback Wing at Transonic Speeds. NACA RM L7F19, 1947.

3. Cahill, Jones F., and Gottlieb, Stanley M.: Low-Speed Aerodynamic Characteristics of a Series of Swept Wings Having NACA 65A006 Airfoil Sections. NACA RM L9J20, 1950.

4. DeYoung, John: Theoretical Additional Span Loading Characteristics of Wings with Arbitrary Sweep, Aspect Ratio, and Taper Ratio. NACA TN 1491, 1947.

TABLE I.- FUSELAGE ORDINATES

[Basic fineness ratio 12; actual fineness ratio 10 achieved by cutting off the rear one-sixth of the body; $\bar{c}/4$ located at $l/2$]

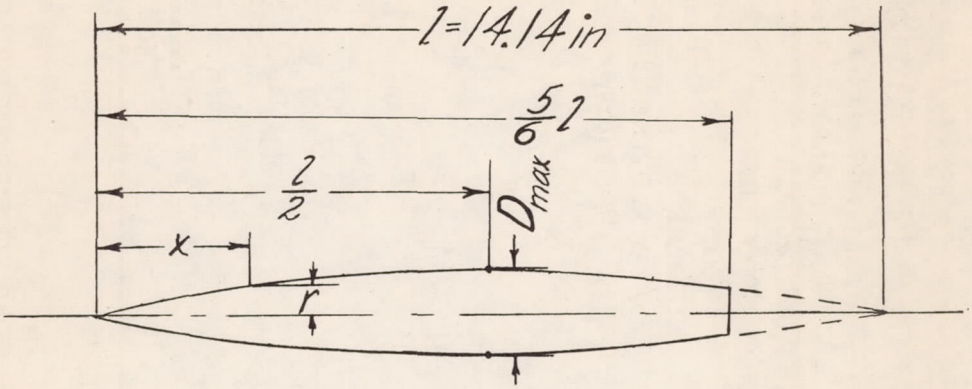

Ordinates			
x/l	r/l	x/l	r/l
0	0	0	0
.005	.00231	.4500	.04143
.0075	.00298	.5000	.04167
.0125	.00428	.5500	.04130
.0250	.00722	.6000	.04024
.0500	.01205	.6500	.03842
.0750	.01613	.7000	.03562
.1000	.01971	.7500	.03128
.1500	.02593	.8000	.02526
.2000	.03090	.8338	.02000
.2500	.03465	.8500	.01852
.3000	.03741	.9000	.01125
.3500	.03933	.9500	.00439
.4000	.04063	1.000	0
L. E. radius = 0.0005l			

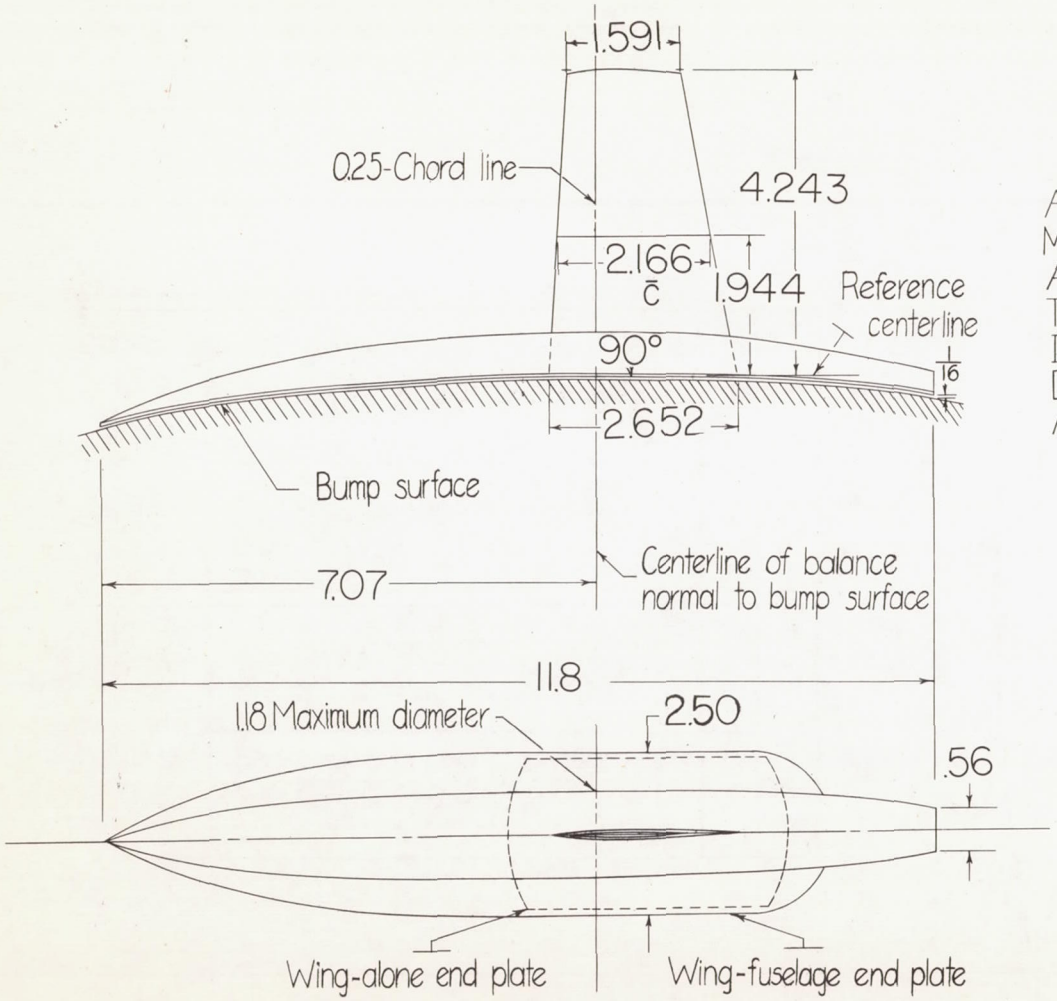

Tabulated Wing Data

Area (Twice semispan)	0.125 sq ft
Mean aerodynamic chord	0.1805 ft
Aspect ratio	4
Taper ratio	0.6
Incidence	0.0°
Dihedral	0.0°
Airfoil section parallel to free stream	NACA 65A004

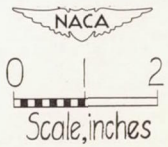

Figure 1.- General arrangement of a model with an unswept wing of aspect ratio 4, taper ratio 0.6, and NACA 65A004 airfoil section.

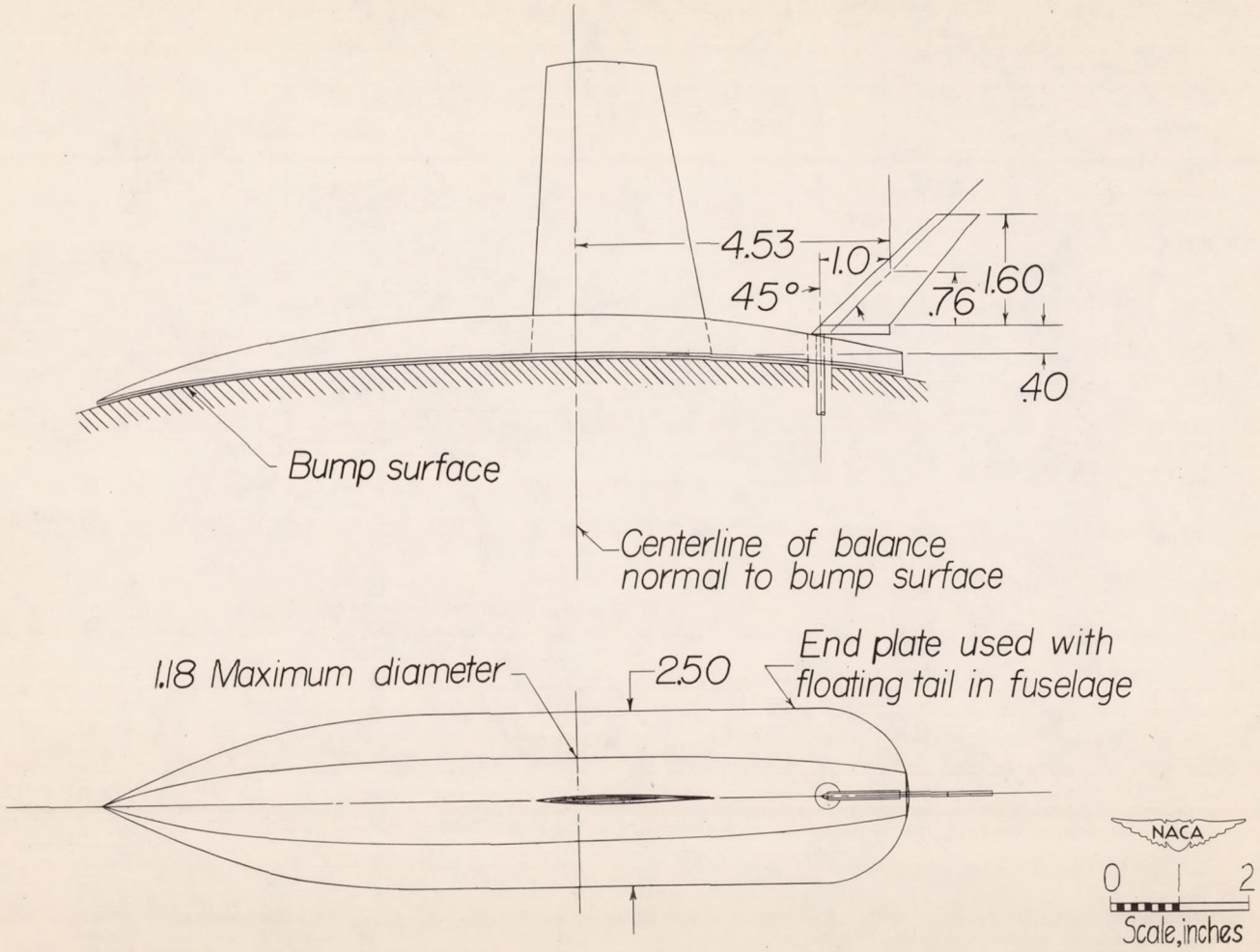

Figure 2.- Details of free-floating tail mounted in fuselage of a model with an unswept wing of aspect ratio 4, taper ratio 0.6, and NACA 65A004 airfoil section.

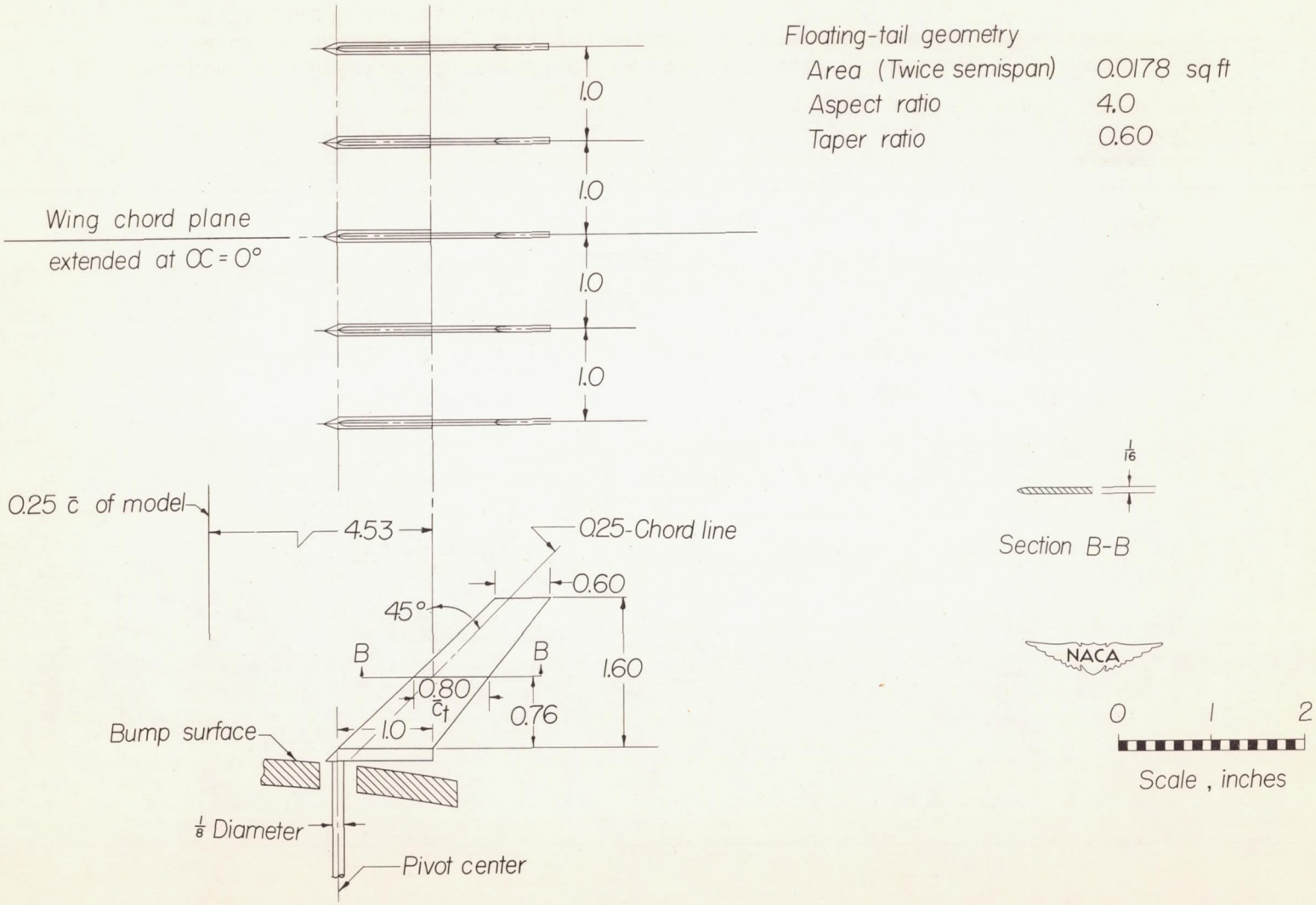

Figure 3.- Details of the free-floating tails used in surveys behind the model.

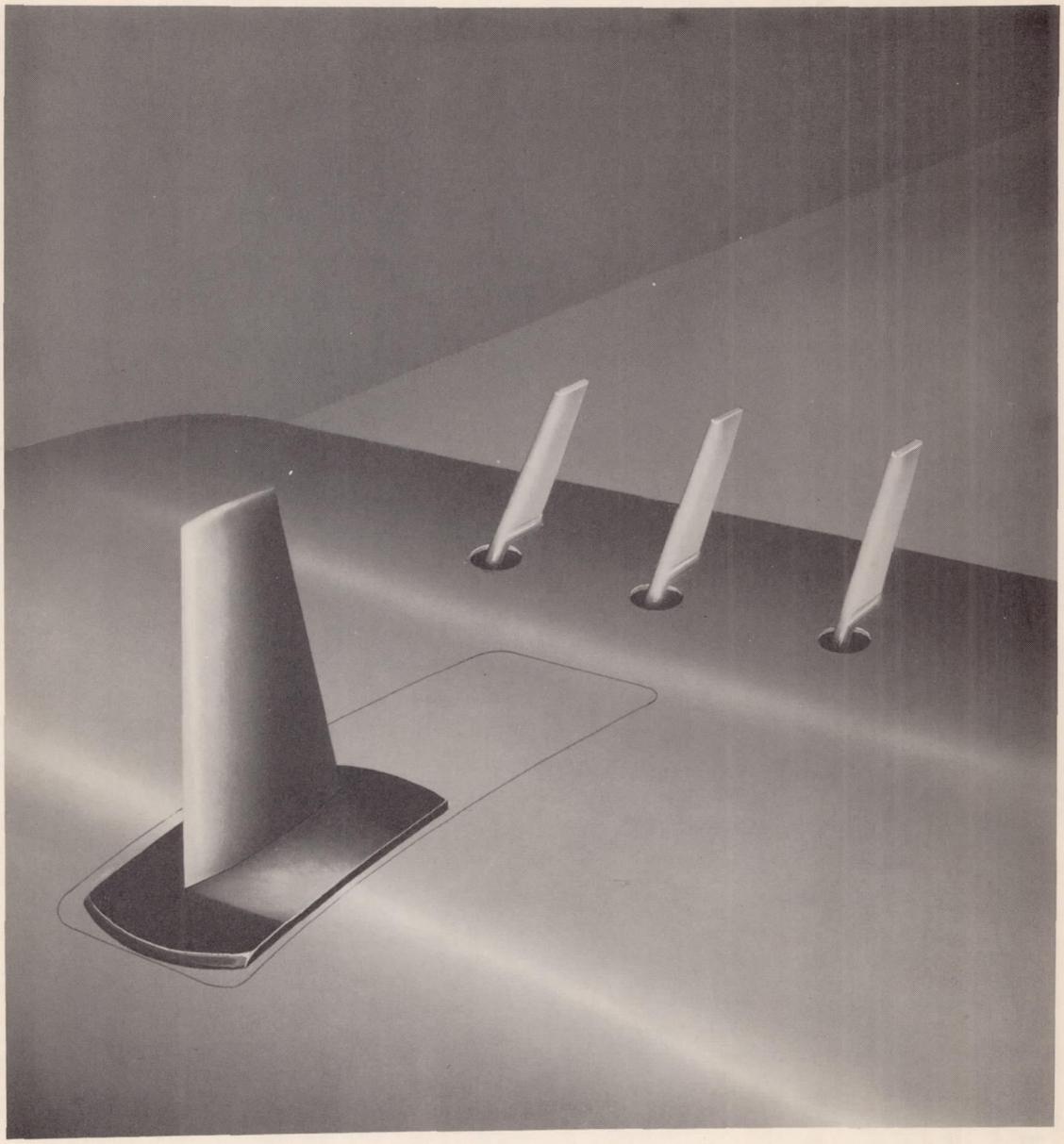

NACA
L-61940.1

Figure 4.- A pictorial view of a model with an unswept wing of aspect ratio 4, taper ratio 0.6, and NACA 65A004 airfoil section mounted on the transonic bump showing free-floating tails.

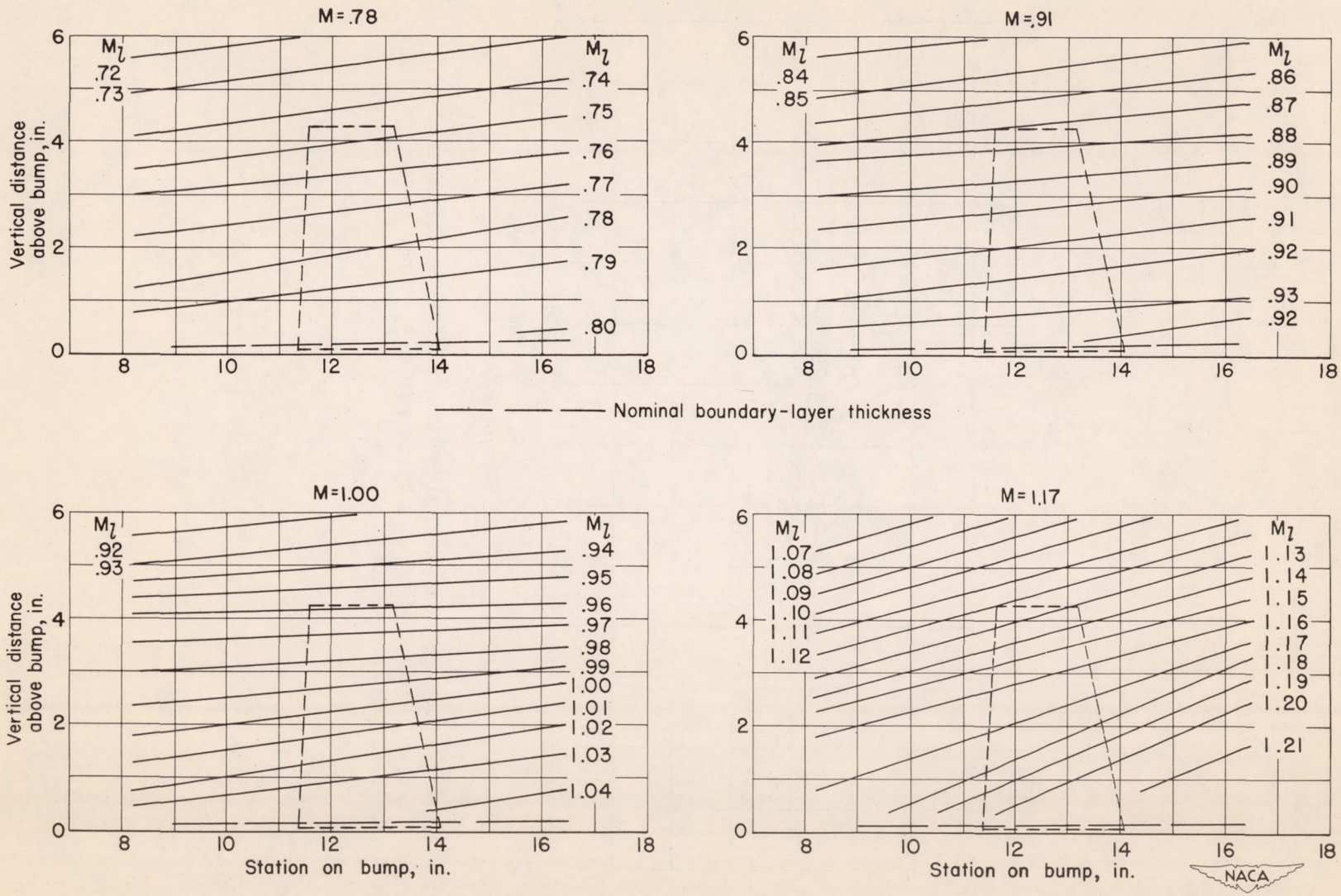

Figure 5.- Typical Mach number contours over transonic bump in region of model location.

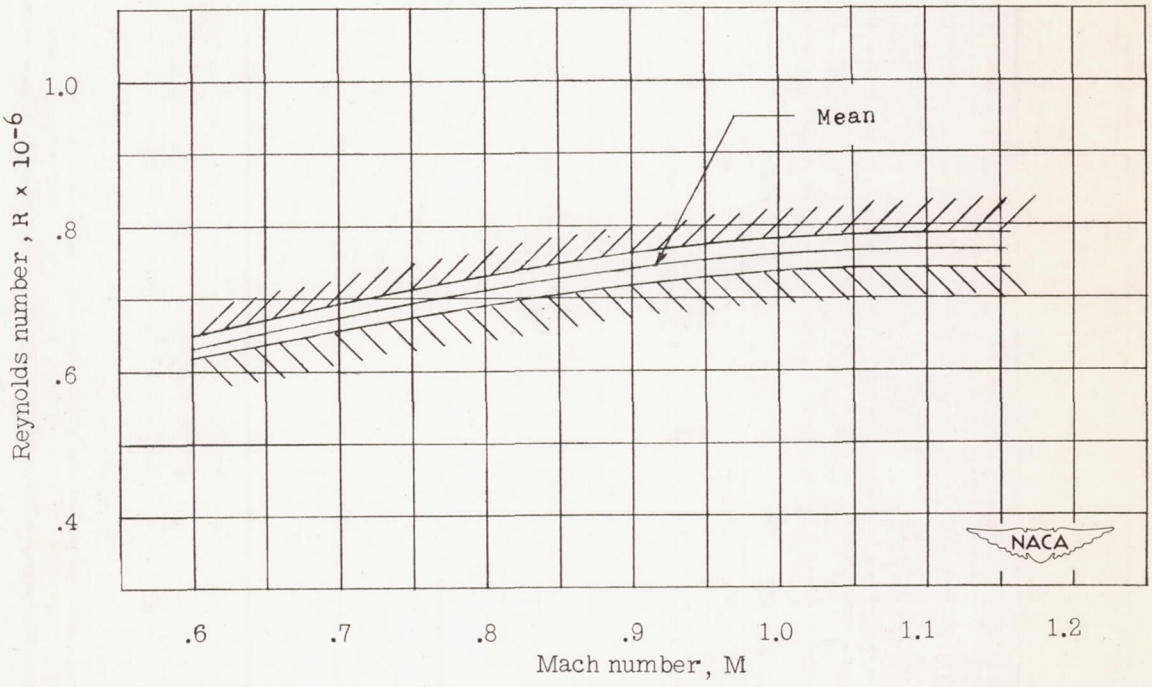

Figure 6.- Variation of test Reynolds number with Mach number for a model with an unswept wing of aspect ratio 4, taper ratio 0.6, and NACA 65A004 airfoil section.

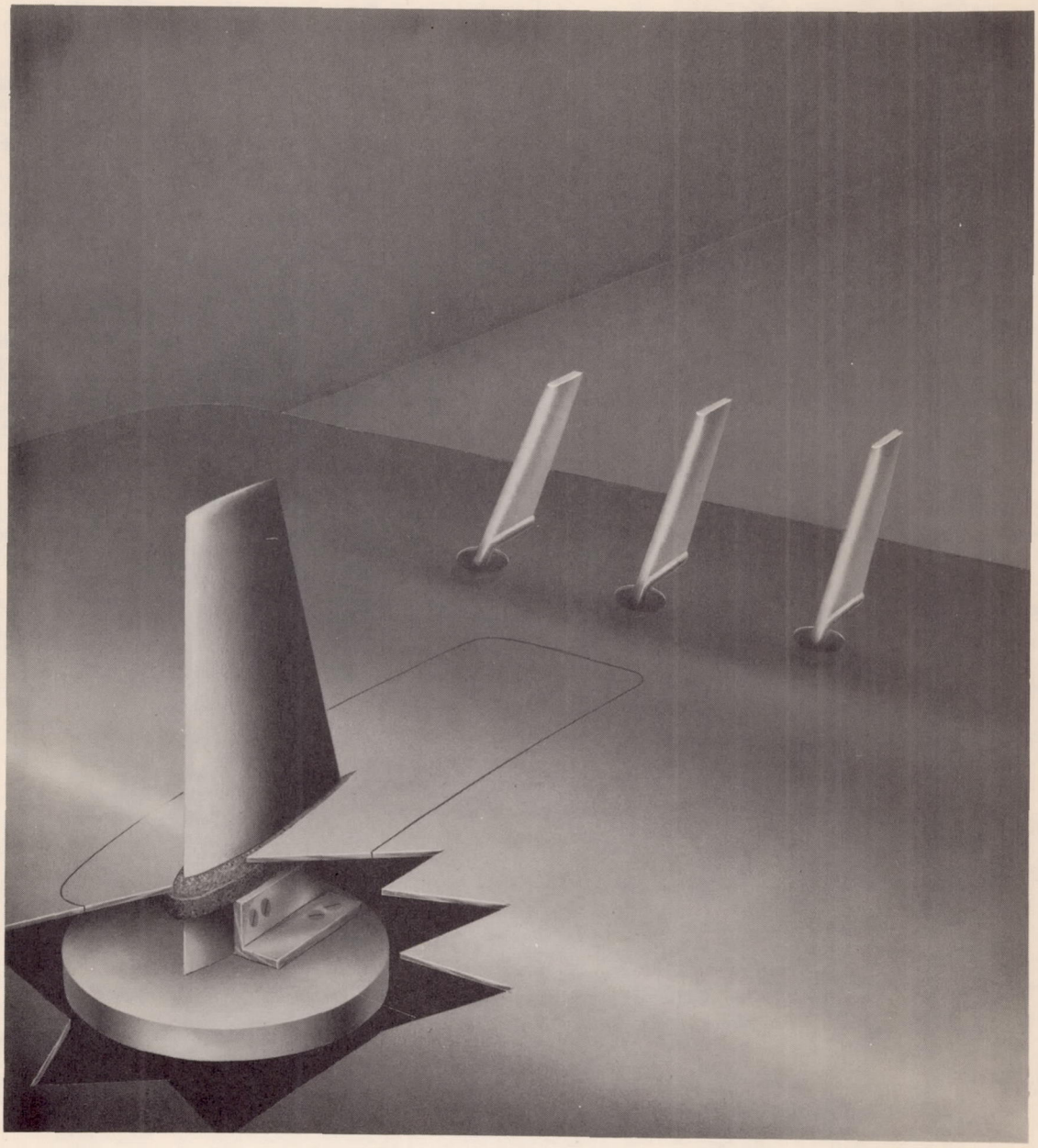

NACA
L-61939.1

Figure 7.- A pictorial view showing sponge-wiper-seal installation on the wing model and position of the free-floating tails.

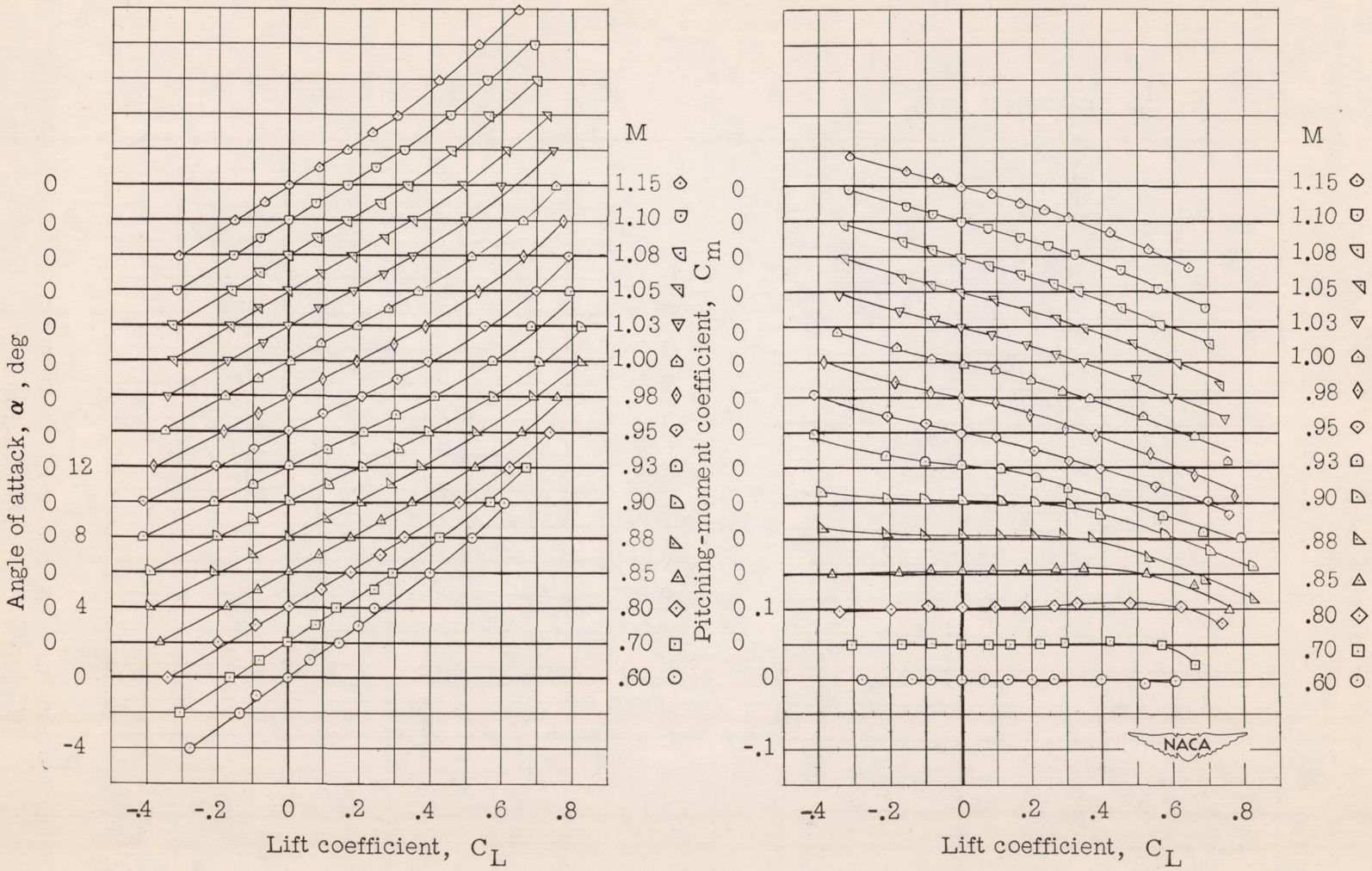

Figure 8.- Aerodynamic characteristics for a model with an unswept wing of aspect ratio 4, taper ratio 0.6, and NACA 65A004 airfoil section. Wing alone.

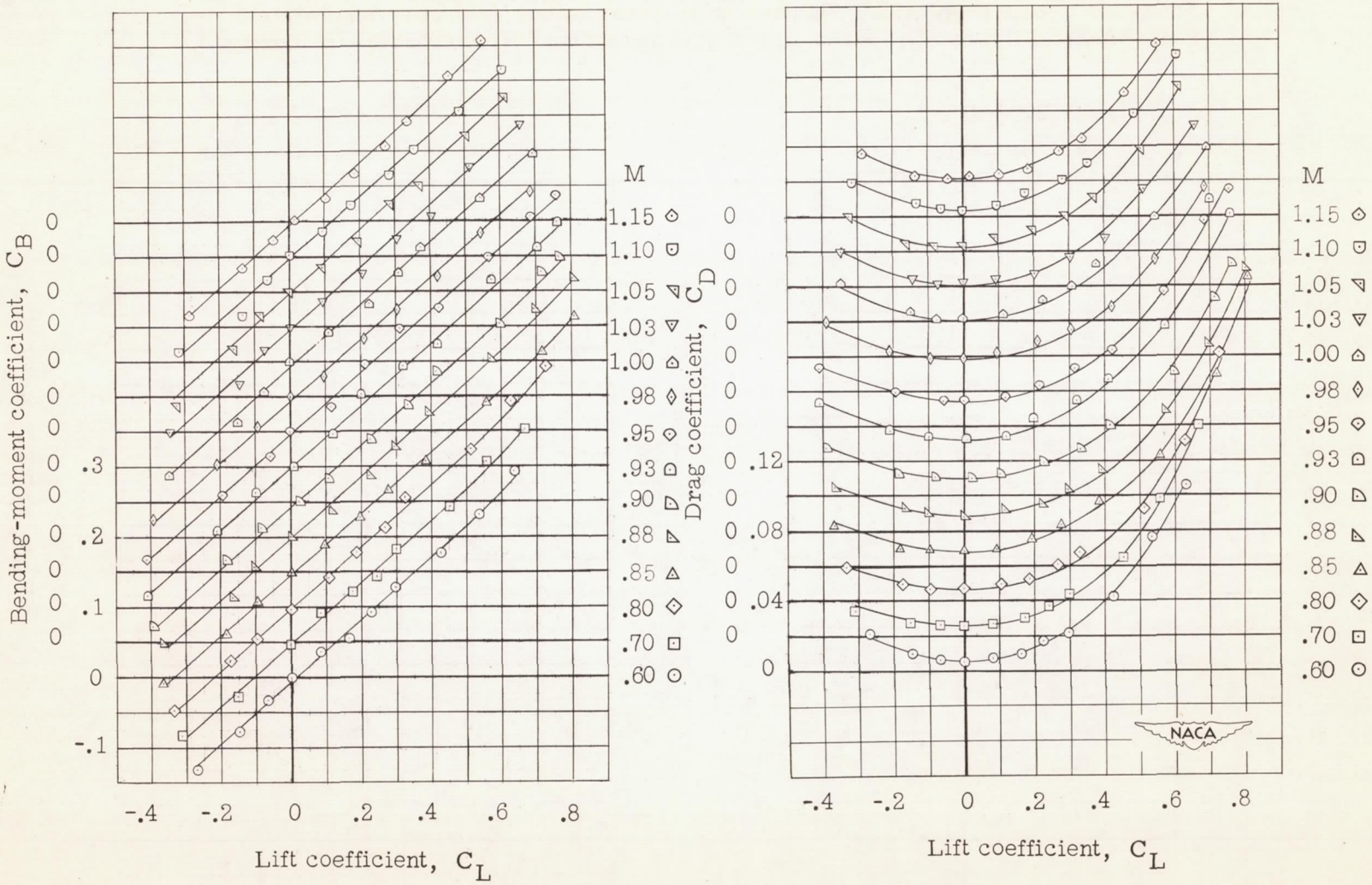

Figure 8.- Concluded.

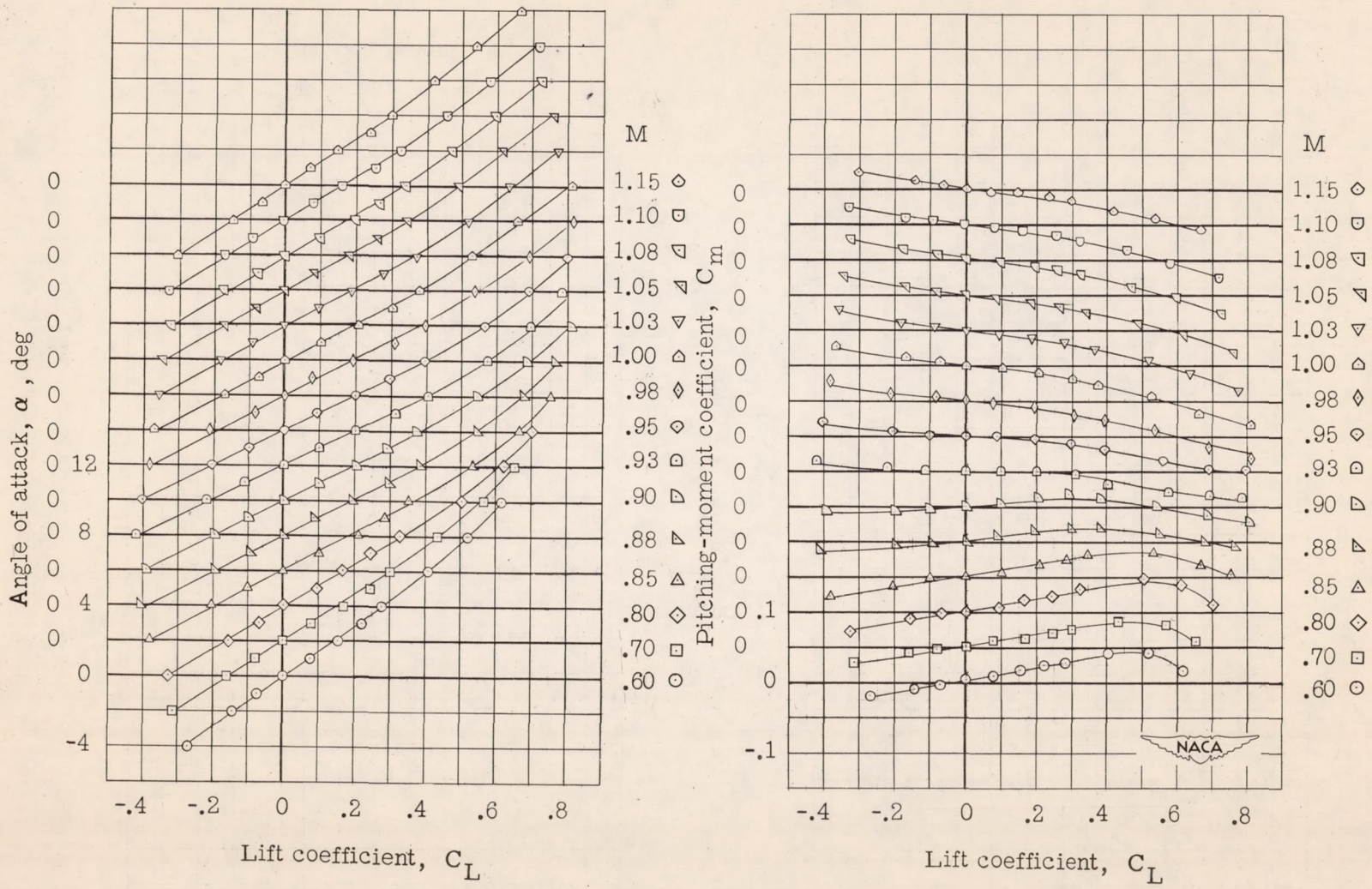

Figure 9.- Aerodynamic characteristics of a model with an unswept wing of aspect ratio 4, taper ratio 0.6, and NACA 65A004 airfoil section. Wing fuselage.

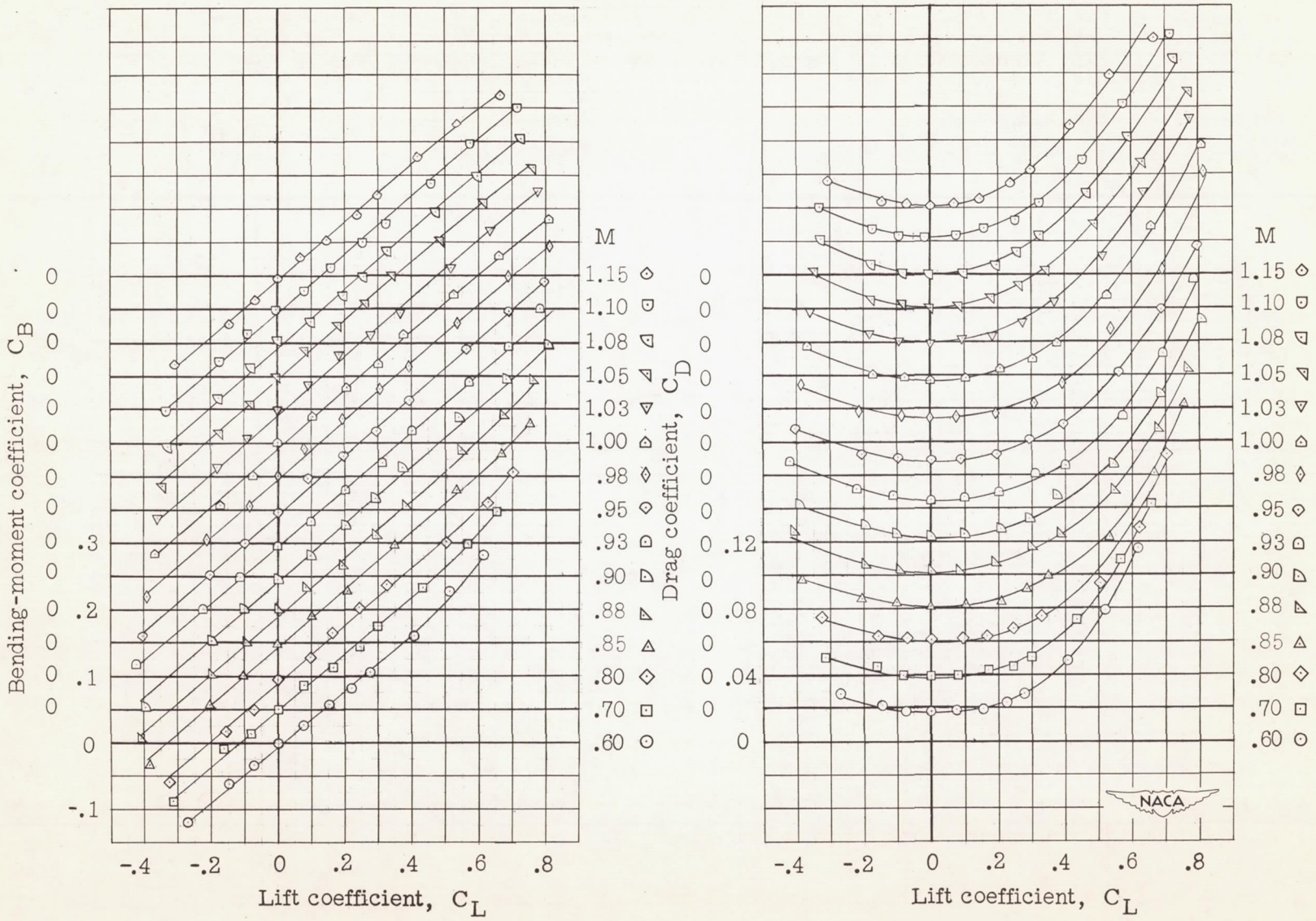

Figure 9.- Concluded.

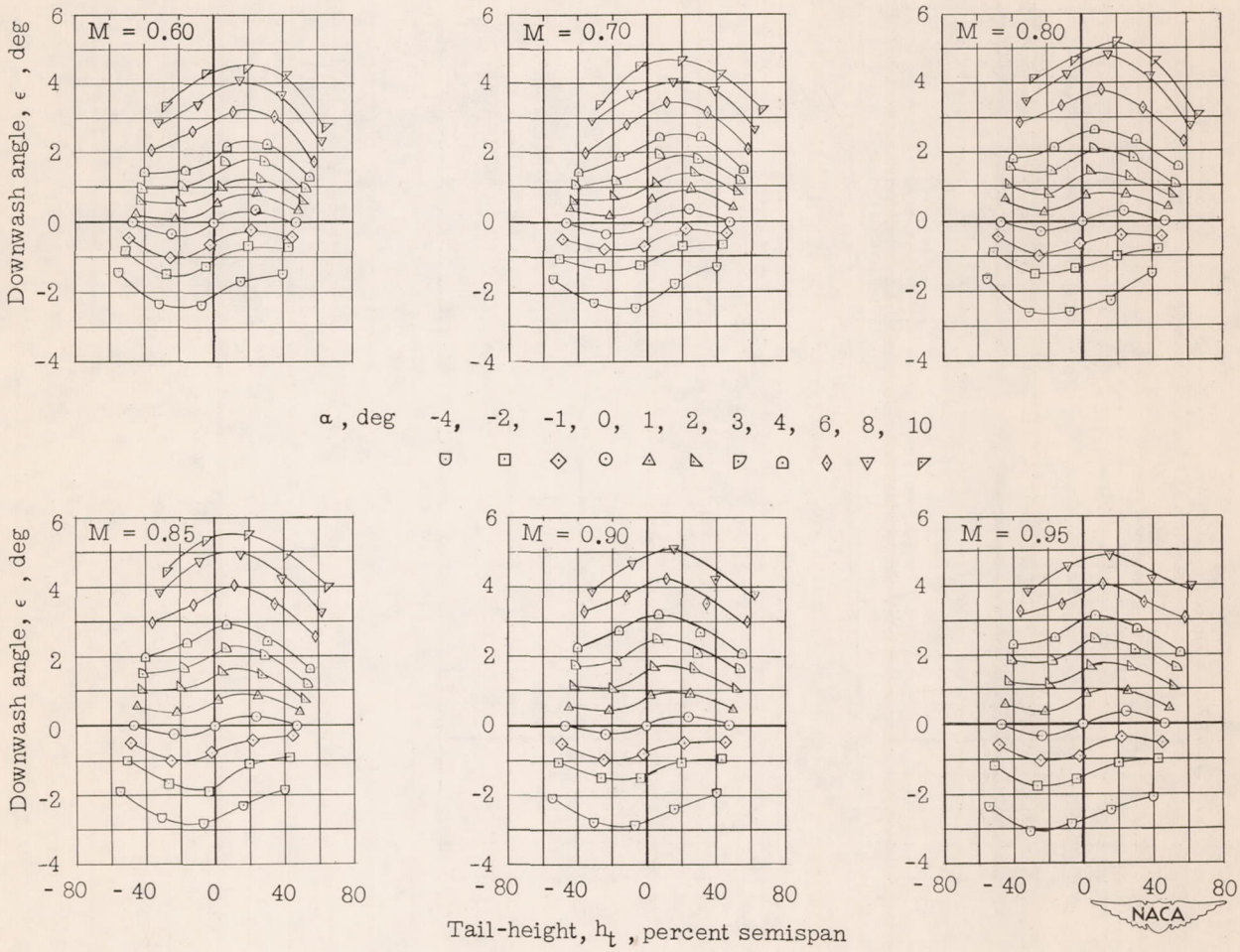

Figure 10.- Effective downwash angles in region of tail plane for a model with an unswept wing of aspect ratio 4, taper ratio 0.6, and NACA 65A004 airfoil section. Wing alone.

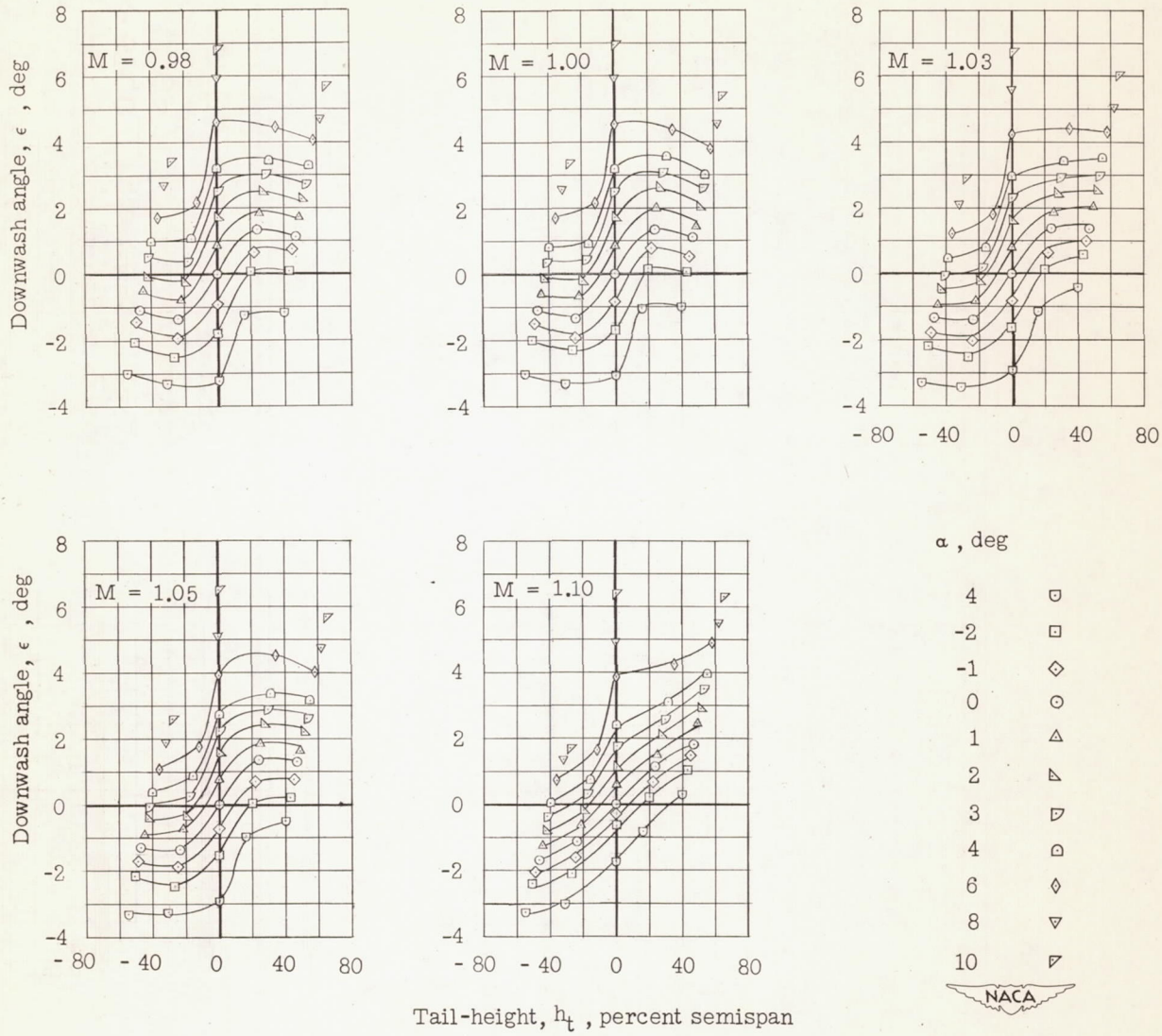

Figure 10.- Concluded.

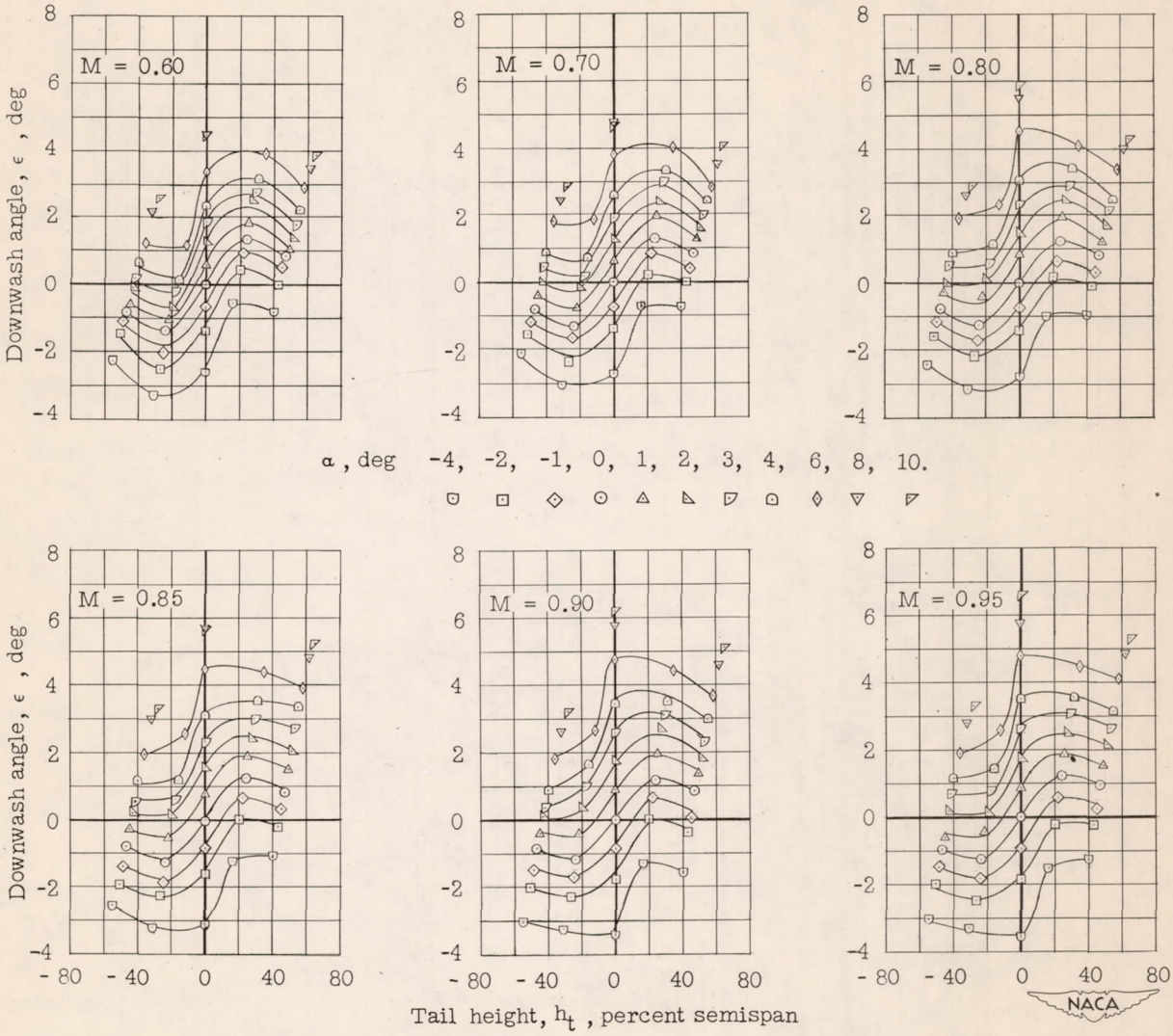

Figure 11.- Effective downwash angles in the region of the tail-plane of a model with an unswept wing of aspect ratio 4, taper ratio 0.6, and NACA 65A004 airfoil section. Wing fuselage.

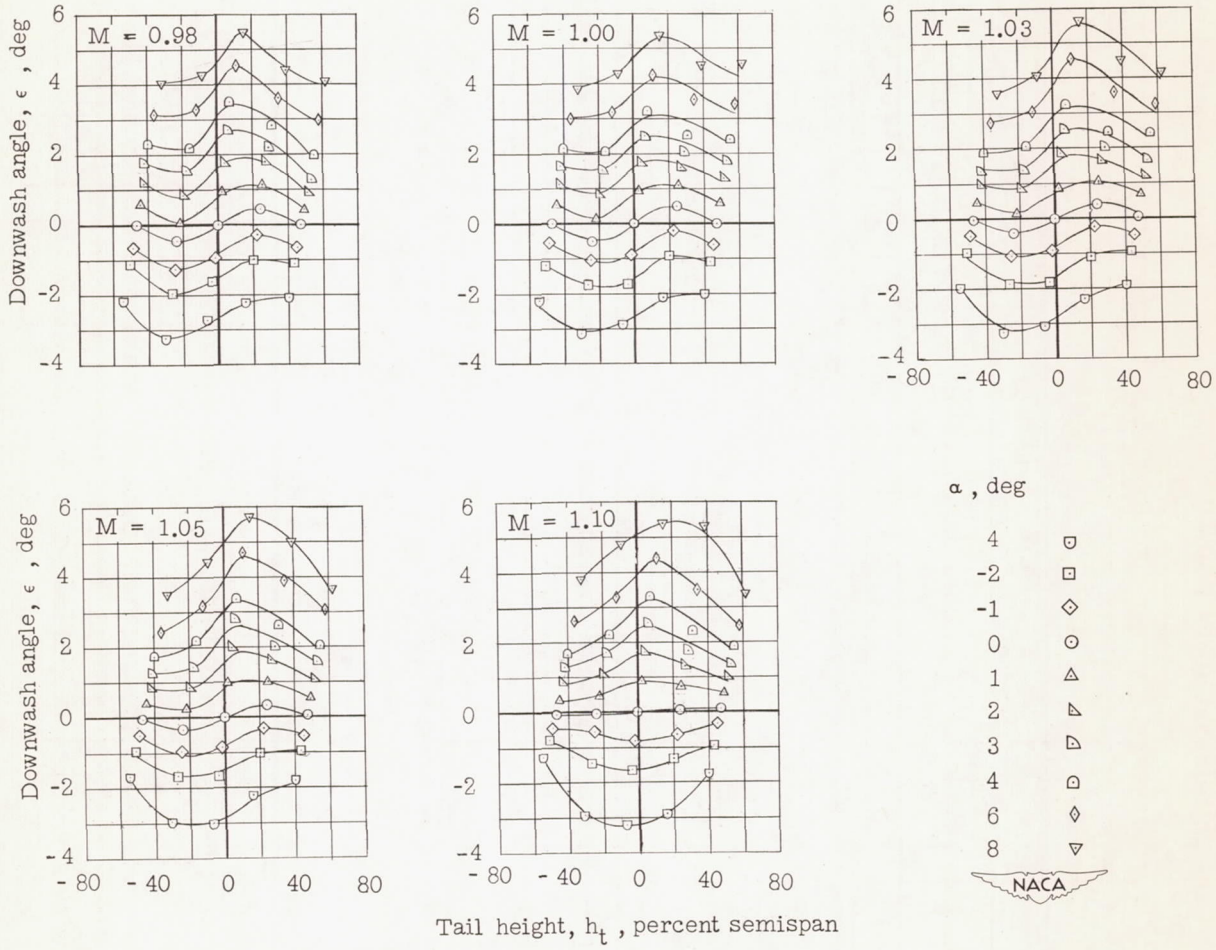

Figure 11.- Concluded.

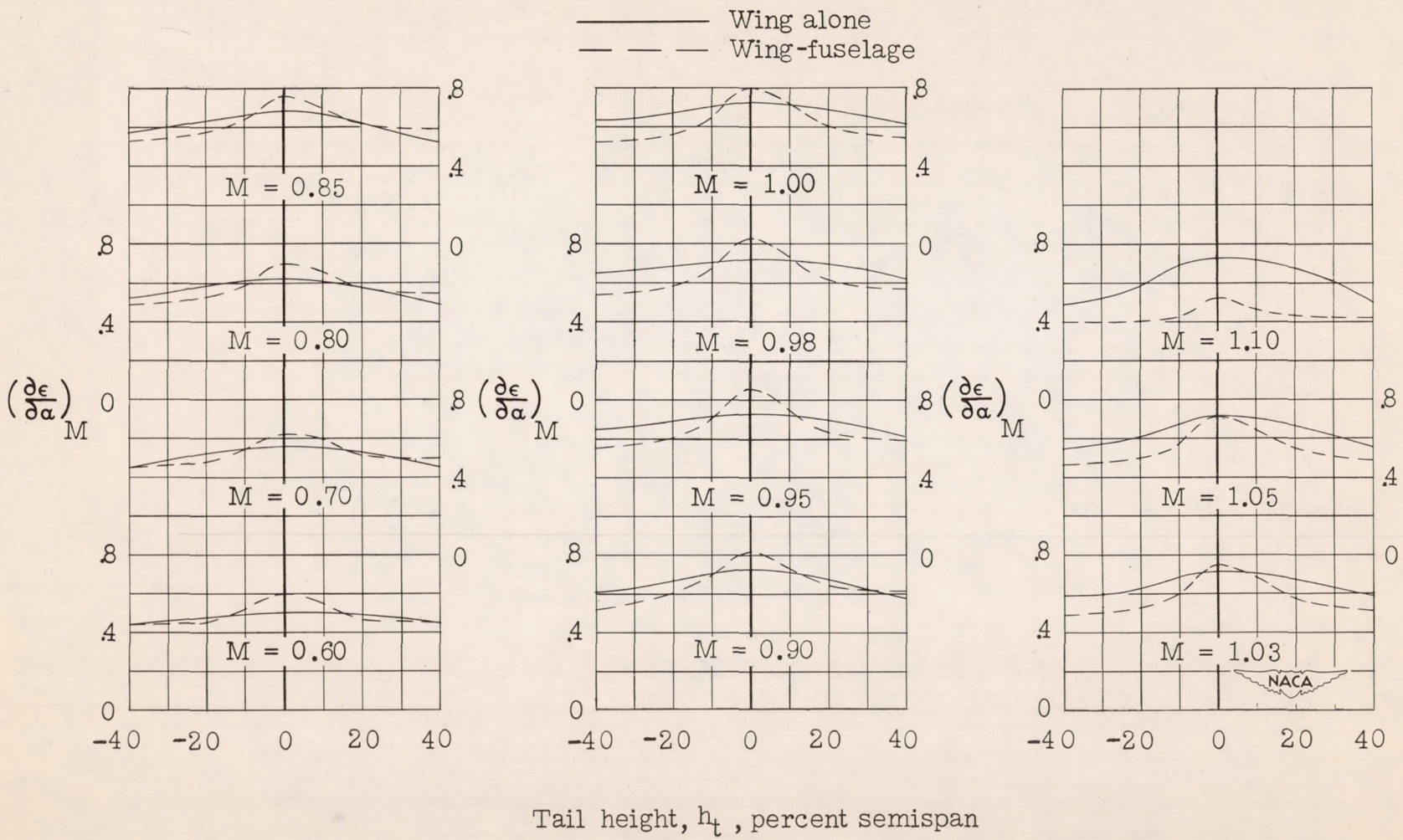

Figure 12.- Variation of downwash gradient with tail height and Mach number for a model with an unswept wing of aspect ratio 4, taper ratio 0.6, and NACA 65A004 airfoil section. $C_L = 0$.

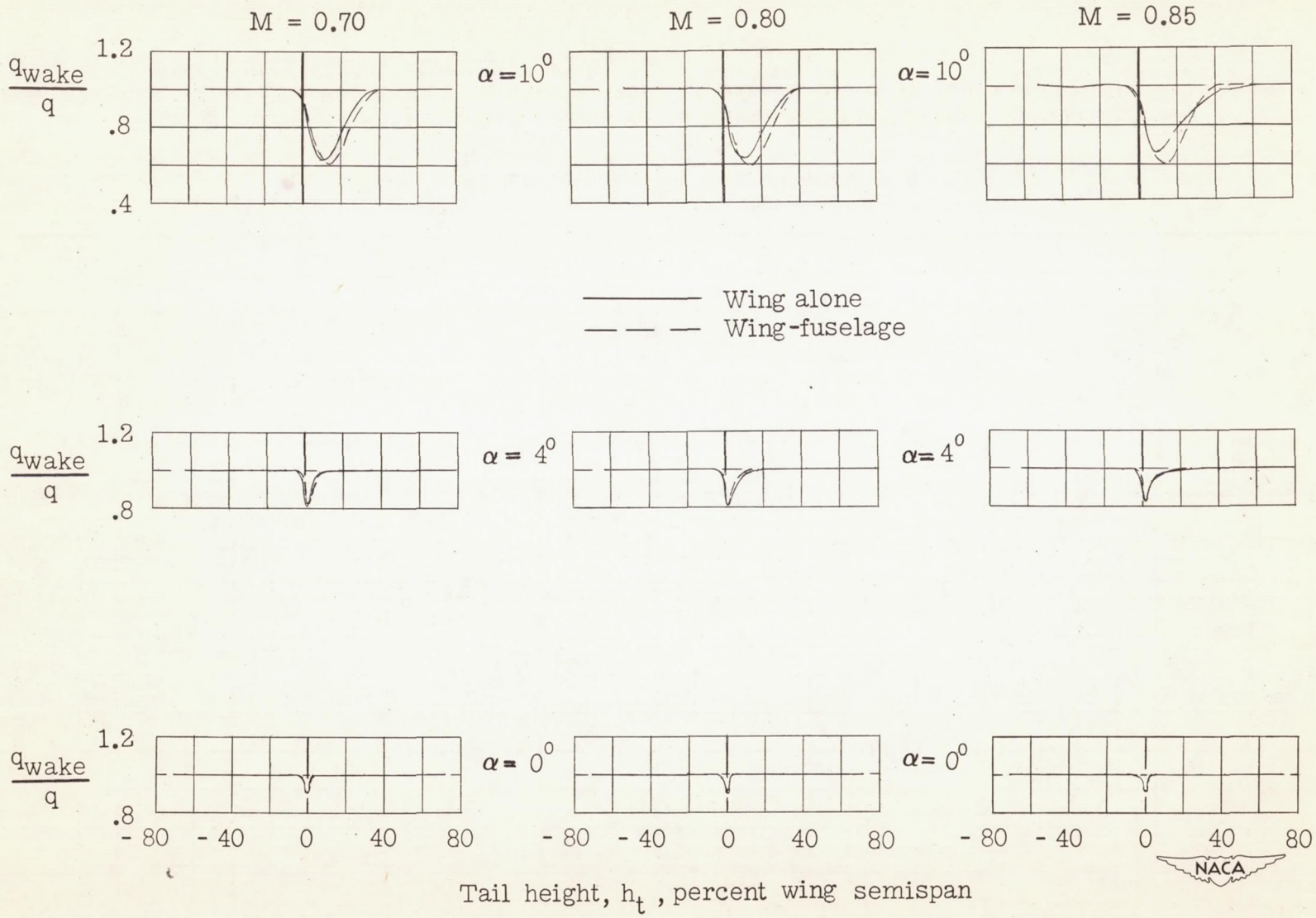

Figure 13.- Dynamic-pressure surveys in region of tail plane for a model with an unswept wing of aspect ratio 4, taper ratio 0.6, and NACA 65A004 airfoil section.

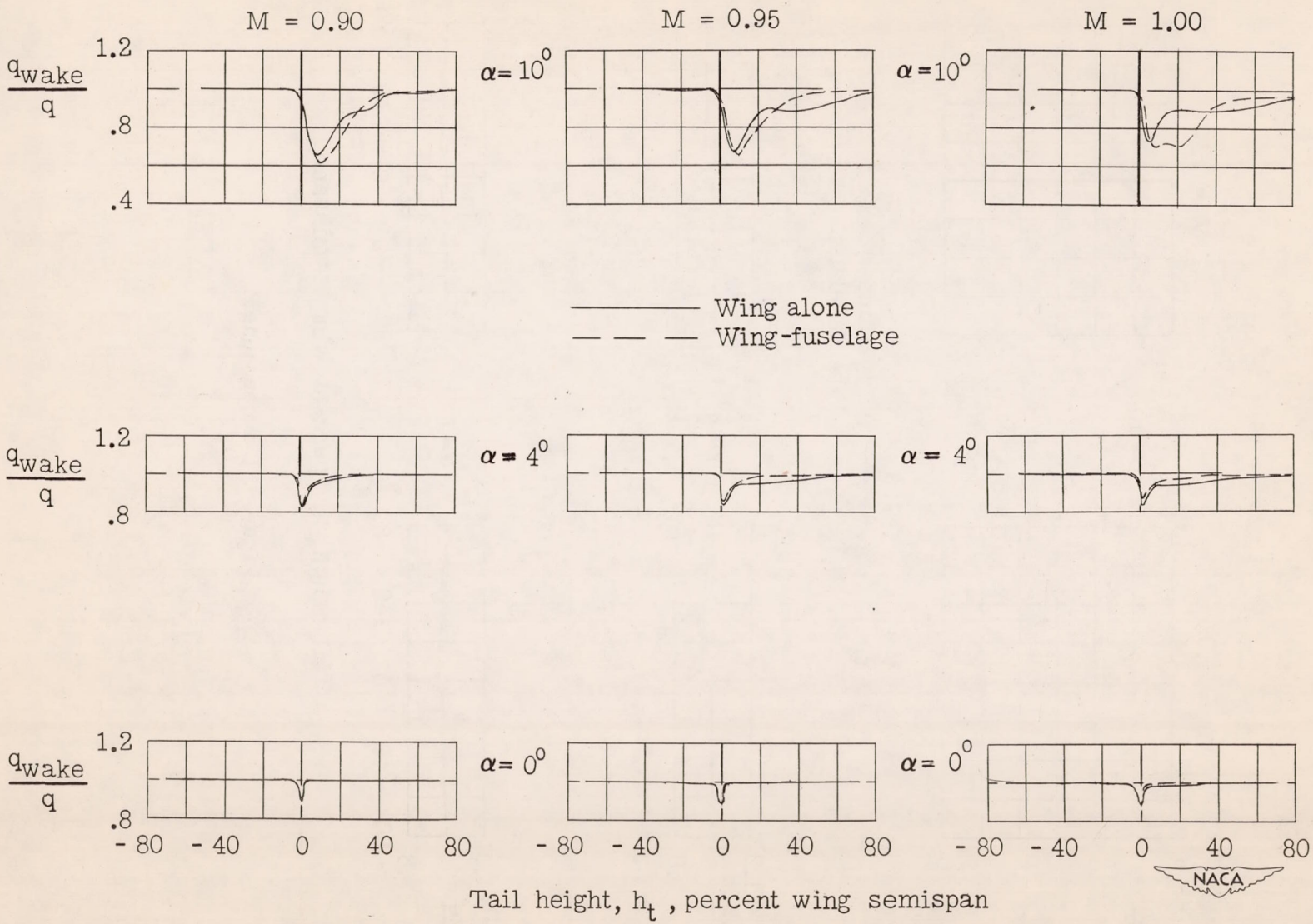

Figure 13.- Continued.

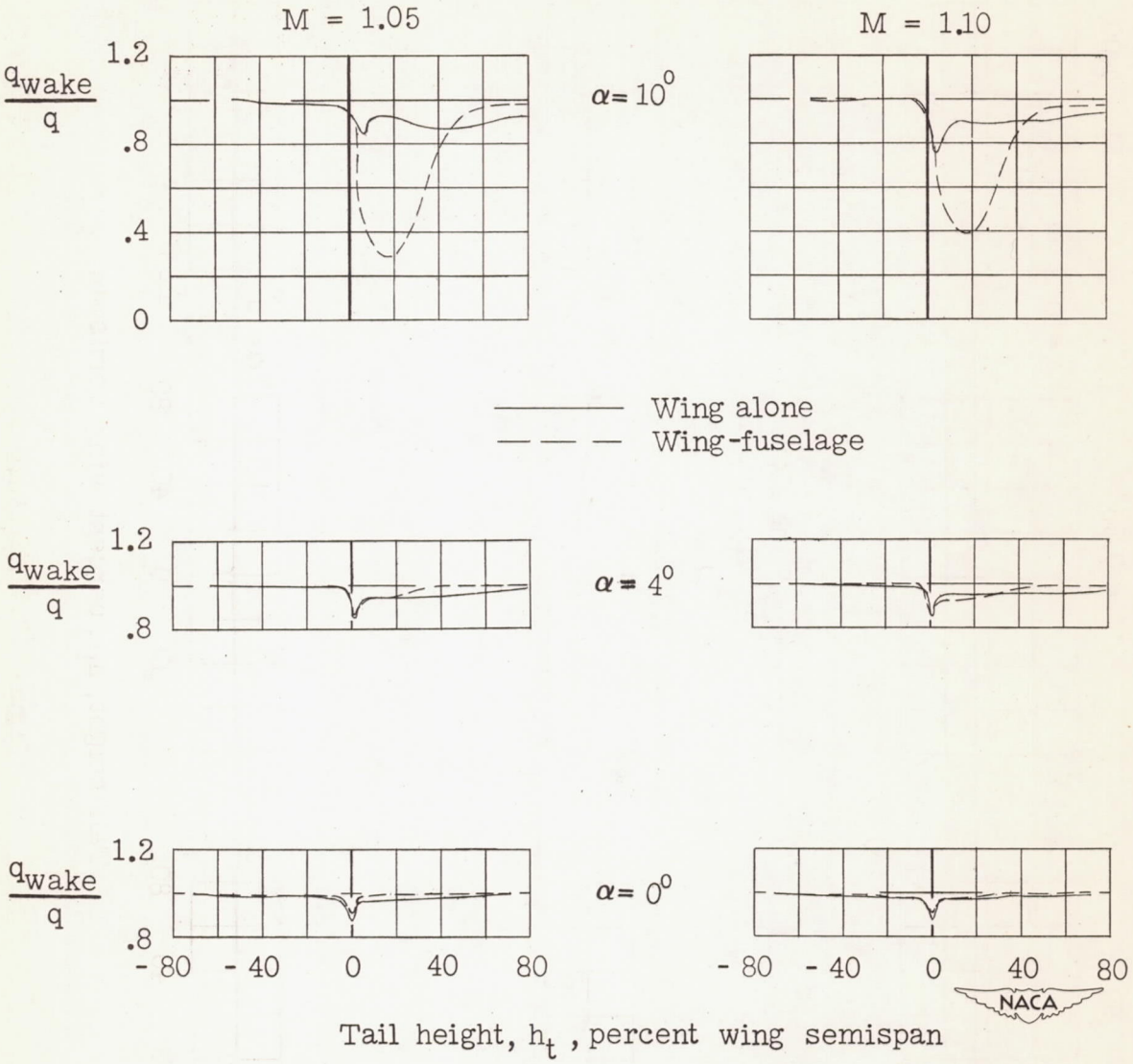

Figure 13.- Concluded.

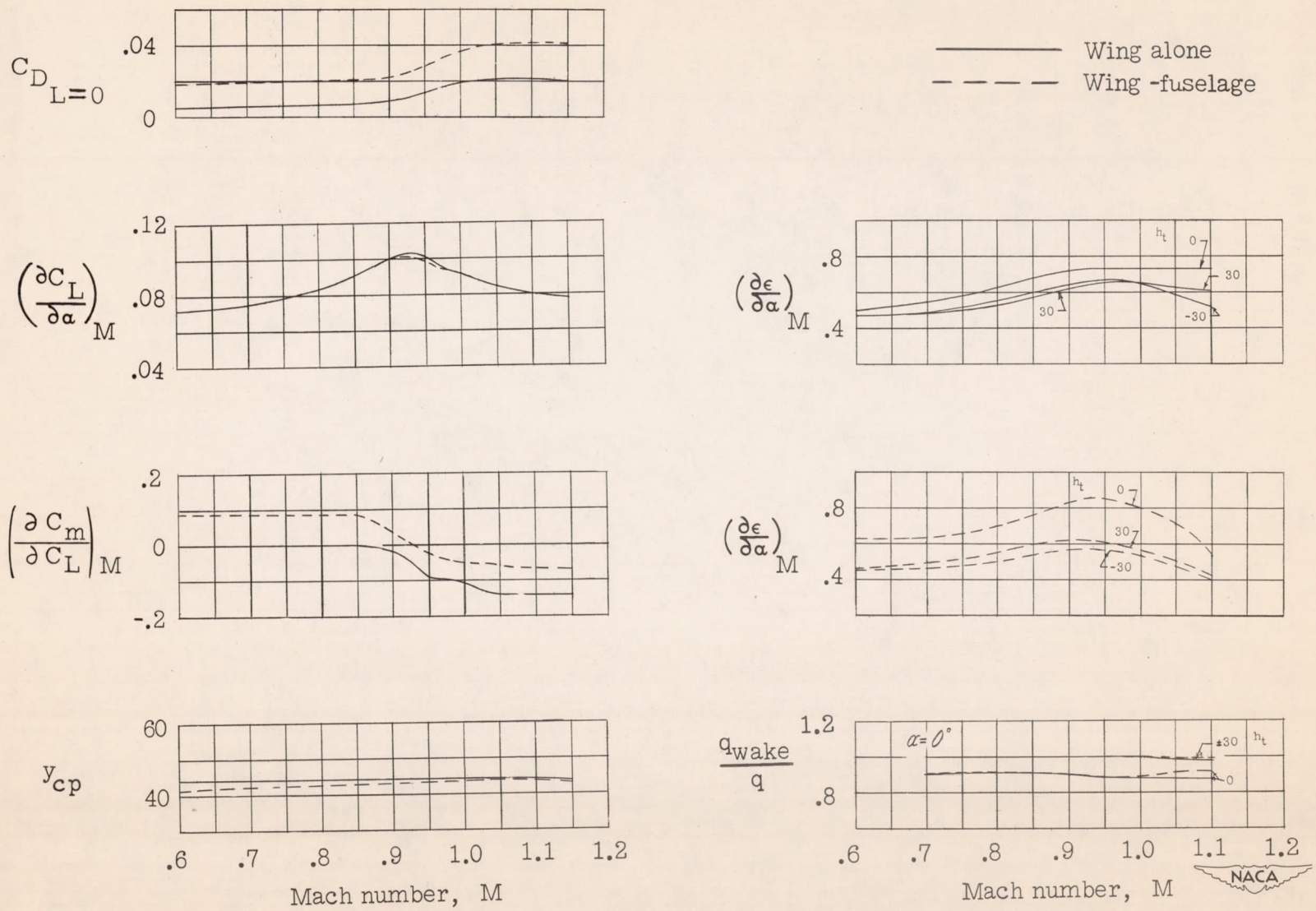

Figure 14.- Summary of aerodynamic characteristics near zero lift for a model with an unswept wing of aspect ratio 4, taper ratio 0.6, and NACA 65A004 airfoil section.

NACA - Langley Field, Va.